Phys. Status Solidi A **214,** No. 8, 1700063 (2017) / **DOI** 10.1002/pssa.201700063

physica status solidi a
www.pss-a.com
applications and materials science

Thermal annealing effect on β-Ga_2O_3 thin film solar blind photodetector heteroepitaxially grown on sapphire substrate

Subrina Rafique, Lu Han, and Hongping Zhao*

Department of Electrical Engineering and Computer Science, Case Western Reserve University, Cleveland, OH 44106, USA

Received 6 February 2017, revised 4 April 2017, accepted 24 April 2017
Published online 12 May 2017

Keywords β-Ga_2O_3 thin films, heteroepitaxy, low pressure chemical vapor deposition, solar-blind photodetectors, ultrawide bandgap

* Corresponding author: e-mail hongping.zhao@case.edu, Phone: 216-368-4120, Fax: 216-368-6888

This paper presents the effect of thermal annealing on β-Ga_2O_3 thin film solar-blind (SB) photodetector (PD) synthesized on c-plane sapphire substrates by a low pressure chemical vapor deposition (LPCVD). The thin films were synthesized using high purity gallium (Ga) and oxygen (O_2) as source precursors. The annealing was performed ex situ the under the oxygen atmosphere, which helped to reduce oxygen or oxygen-related vacancies in the thin film. Metal/semiconductor/metal (MSM) type photodetectors were fabricated using both the as-grown and annealed films. The PDs fabricated on the annealed films had lower dark current, higher photoresponse and improved rejection ratio (R_{250}/R_{370} and R_{250}/R_{405}) compared to the ones fabricated on the as-grown films. These improved PD performances are due to the significant reduction of the photo-generated carriers trapped by oxygen or oxygen-related vacancies.

1 Introduction Deep-ultraviolet (DUV) solar-blind (cut-off wavelength <280 nm) photodetectors (PDs) have received considerable research attention due to their applications in both military and civil surveillance such as missile tracking, secure communication, ozone hole monitoring, flame detection, and chemical/biological analysis [1]. Conventional Si and GaAs based DUV PDs require additional visible light blocking filters which are fragile, bulky, costly, and are operational only under large bias conditions [2]. As a result, solid state PDs based on ultrawide bandgap semiconductors such as AlGaN [3], ZnMgO [4], and diamond [5] are regarded as promising candidates for DUV detection. However, challenges still exist for these materials to be applicable for DUV PDs, such as high defects in AlGaN with high Al-content to achieve a large bandgap [6], a phase segregation between the wurtzite ZnO and the rock salt MgO under Mg rich conditions [7], and for diamond, it is costly and its detection range is constrained to below 225 nm due to a fixed bandgap of ~5.5 eV [8].

Monoclinic β-Ga_2O_3 is a promising candidate for DUV PD because of its desirable properties such as a bandgap of ~4.9 eV and an excellent chemical, mechanical and thermal stability [9]. Due to their intrinsic solar-blindness, PDs based on β-Ga_2O_3 do not require any supplementary filter. They can also avoid the alloying thus, simplifying the material growth process. Many studies of Ga_2O_3 based solar-blind PDs have appeared in recent years. Ga_2O_3 nanomaterials [10–13], thin films [14–18], and single crystals [19–21] have been used as the active layers for such PDs. Methods to synthesize β-Ga_2O_3 thin films include the molecular beam epitaxy (MBE) [22], the metal organic vapor phase epitaxy (MOVPE) [23], the halide vapor phase epitaxy (HVPE) [24], and the low pressure chemical vapor deposition (LPCVD) [25–27]. Various types of PDs such as schottky [28, 29], metal/semiconductor/metal (MSM) [30–32], and p-n heterojunction [33–35] have been reported so far.

In this article, β-Ga_2O_3 thin films were synthesized on a c-plane sapphire substrate by LPCVD. The details of the growth process were reported elsewhere [25–27]. The thin films were annealed ex situ in oxygen at 1000 °C for 1 hr. The MSM PDs were fabricated on both the as-grown and the

annealed β-Ga_2O_3 thin films using standard photolithography and lift-off processes. Ti/Au (80 nm/120 nm) interdigital electrodes were deposited by thermal evaporation to form an ohmic contact [1]. The electrodes were 1500 μm long, 100 μm wide, and had a100 μm spacing gap. Both the crystal qualities and the device performances of the fabricated MSM PDs were comparatively studied based on the as-grown and annealed β-Ga_2O_3 thin films. Our findings demonstrated that the performance of the PD fabricated on the annealed thin film is superior to the one on the as-grown thin film.

2 Material characterization The surface morphology, the crystal quality and optical properties of the heteroepitaxial β-Ga_2O_3 thin films were characterized by using scanning electron microscopy (SEM), X-ray diffraction (XRD), and photoluminescence (PL) spectroscopy. The SEM images were taken with Tescan Vega-3 SBH. XRD spectra were collected on a Bruker Discover D8 X-Ray Diffractometer with Cu Kα radiation (1.54 Å). PL spectra were measured using a Jobin Yvon-spex-Fluorog-3-Spectrofluorimeter. X-ray photoelectron spectroscopy (XPS) was collected on a Phi versaprobe 5000 scanning XPS spectrometer. The current-voltage (*I–V*) characteristics and the time-dependent photoresponse of the β-Ga_2O_3 thin films based MSM PDs were measured by Keithley 4200 SCS. The photoresponse measurement was performed with a 0.1 mW excitation power UV light emitting diode (LED) of 250 nm wavelength as the light source. All the measurements were performed in air at room temperature.

3 Results and discussion To illustrate the effect of thermal annealing on the surface topography of β-Ga_2O_3 thin films, Fig. 1 shows the top view SEM images of both as-grown and annealed β-Ga_2O_3 thin films synthesized on c-plane sapphire substrates at 900 °C. The as-grown thin film is composed of small pseudo hexagonal rotational domains. The well-defined grain boundaries are clearly visible in the SEM image of Fig. 1(a). However, the annealed film has a smoother surface morphology and a relatively larger feature size. To further corroborate our conclusion from SEM, AFM measurements were conducted on both as-grown and annealed β-Ga_2O_3 thin films. Figure 1(c and d) show the AFM images of a 5 × 5 μm scan for the as-grown and annealed thin films, respectively. The surface RMS roughnesses for the as-grown and annealed thin films were 10.1 and 6.87 nm, respectively. This demonstrates that the small grain islands have been merged into large crystalline grains due to the supply of sufficient thermal energy.

The influence of thermal annealing on the crystal quality of the β-Ga_2O_3 thin films was characterized by XRD and a rocking curve measurement. From XRD θ–2θ scan spectrum of the as-grown β-Ga_2O_3 thin film (not shown), besides the (0006) diffraction peak of the substrate, only reflections from (−201) family of the planes of β-Ga_2O_3 are present in the spectrum. This indicates that the as-synthesized thin film has (−201) as the preferred growth orientation [36]. Figure 2 shows the XRD rocking curves of the (−201) diffraction peaks of the as-grown and annealed β-Ga_2O_3 thin films. The full widths at half maximum (FWHM) of the rocking curves are measured as 1.883° (as-grown) and 1.853° (annealed),

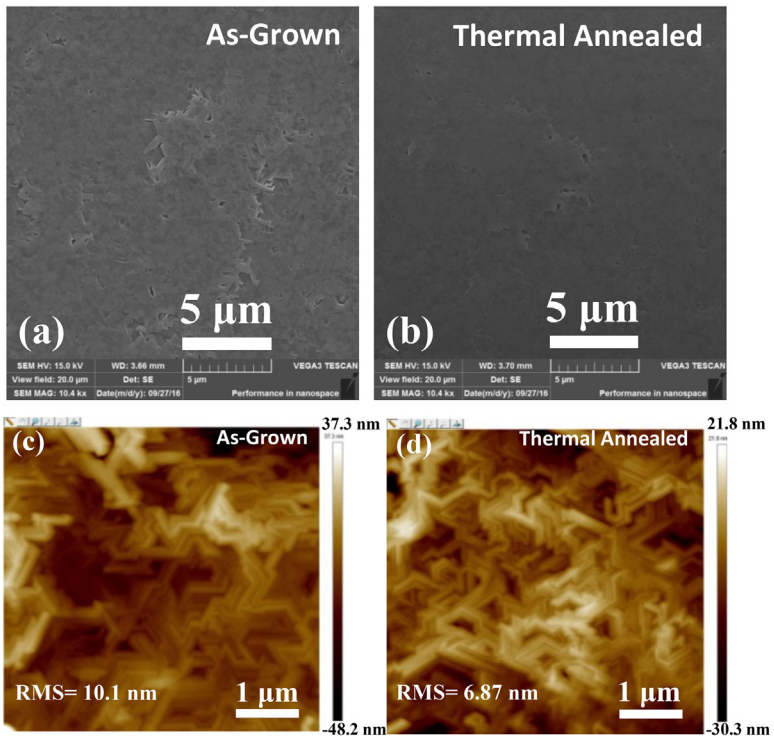

Figure 1 Top view SEM images of (a) as-grown and (b) thermal annealed β-Ga_2O_3 thin films grown on a c-plane sapphire substrate. Surface AFM images (5 × 5 μm) of (c) as-grown and (d) thermal annealed β-Ga_2O_3 thin films.

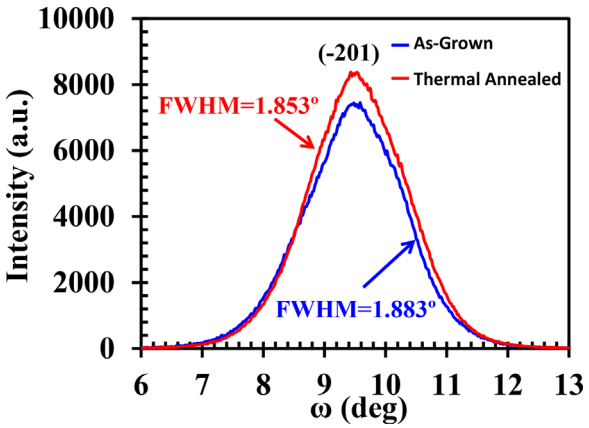

Figure 2 XRD rocking curves of (−201) peak reflection of as-grown and thermal annealed β-Ga_2O_3 thin films.

respectively. The narrowing of the FWHM value indicates that annealing did not degrade the crystal quality of the β-Ga_2O_3 thin films.

MSM PDs were fabricated on both the as-grown and the annealed β-Ga_2O_3 thin films to study the UV photoresponse. Figure 3(a) shows the schematic illustration of the fabricated PD. Figure 3(b and c) shows the *I–V* characteristics of both types of PDs under the dark and the illumination with 250, 370, 405, and 465 nm wavelengths. Under a 250 nm illumination, the current increased from 0.33 to 1160 nA at a bias voltage of 1 V for the PD fabricated on the as-grown β-Ga_2O_3 thin film. In contrast, the currents were 8.1, 2.4, and 2.9 nA under the 370, 405, and 465 nm illumination, respectively. The defect levels within the bandgap were responsible for the PD response to the sub-bandgap illuminations. For the PD fabricated on annealed β-Ga_2O_3 thin film, the dark current was below the instrument measurement limit and the current under a 250 nm illumination was 1415 nA at 1 V bias voltage. The currents corresponding to the sub-bandgap illumination was also reduced significantly after annealing. The performances of the PDs calculated at 1 V bias voltage are summarized in Table 1. The PD fabricated on the annealed β-Ga_2O_3 thin film exhibited superior performance compared to the one fabricated on as-grown β-Ga_2O_3 thin film which is due to

Table 1 Device characteristics of the PDs fabricated on as-grown and annealed β-Ga_2O_3 thin films.

	I_{250}/I_{dark}	R_{250} (A/W)	rejection ratio (R_{250}/R_{370})	rejection ratio (R_{250}/R_{405})
as-grown	3.5×10^3	0.11	1.47×10^2	4.47×10^2
annealed	1.44×10^6	0.14	8.4×10^4	4.4×10^5

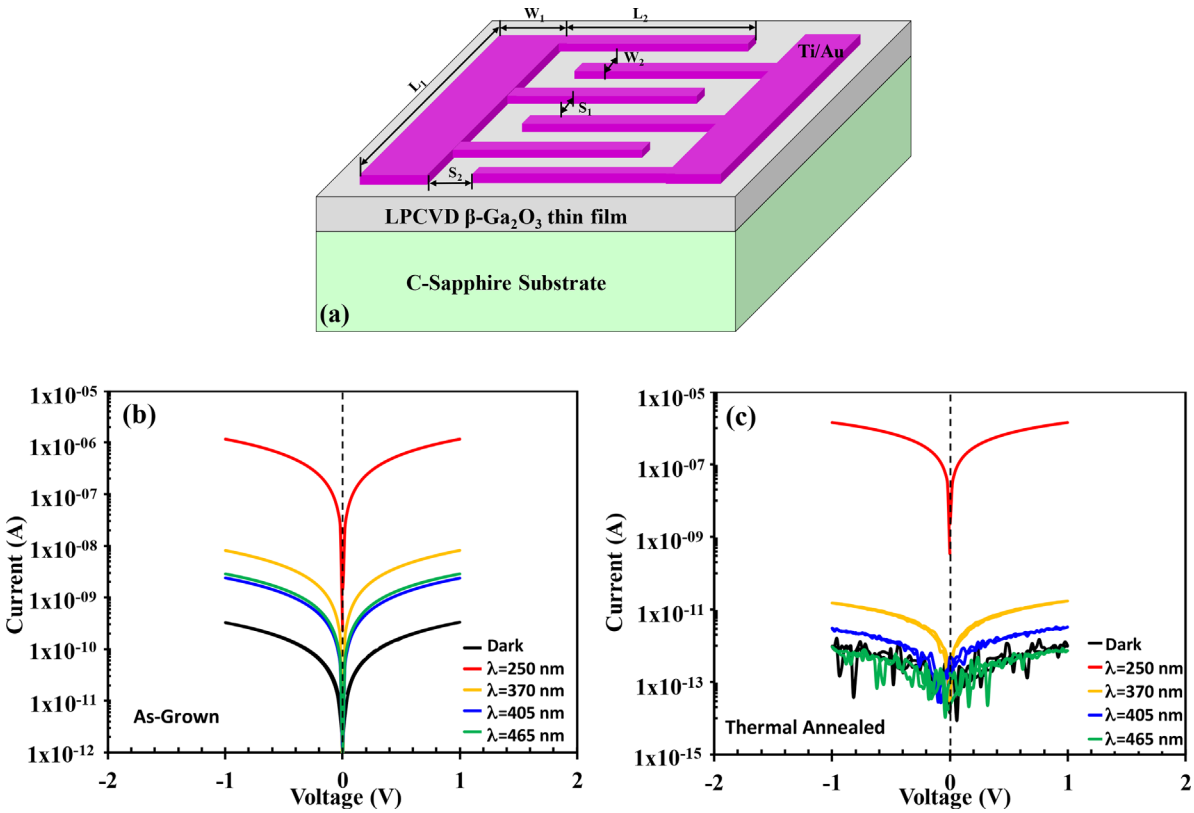

Figure 3 (a) Schematic diagram of the Ga_2O_3 thin film MSM type photodetector. (b) *I–V* characteristics curves of (b) as-grown and (c) thermal annealed β-Ga_2O_3 thin film photodetectors in the dark, and under $\lambda = 250$ nm, 370, 405, and 465 illumination.

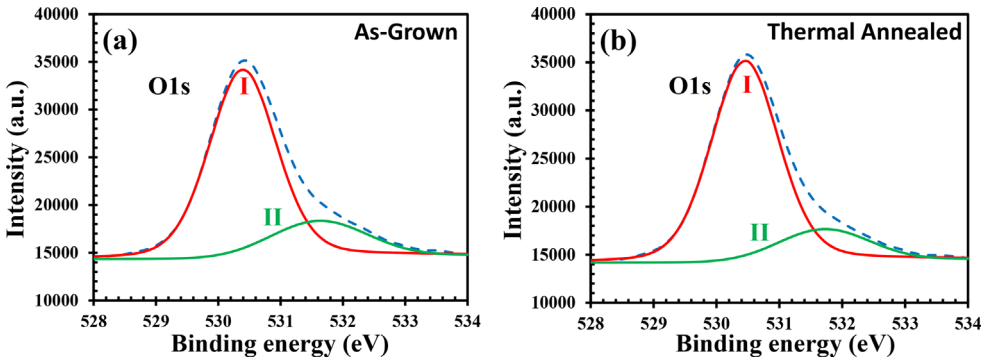

Figure 4 O 1s XPS spectra of the as-grown and thermal annealed β-Ga_2O_3 thin films.

the improved material quality after annealing. Thermal annealing reduced the sub-bandgap defects and made the PD more sensitive to the 250 nm illumination than to the 370 and 405 nm illumination.

To investigate the mechanism of the lower dark current for the PDs fabricated on annealed β-Ga_2O_3 thin films, XPS was conducted. Figure 4 shows the XPS spectra of O 1 s peaks of both as-grown and annealed β-Ga_2O_3 thin films. The peak can be divided into two components (I and II). Peak II is usually associated with oxygen or oxygen-related vacancies [37–39]. The area of peak II was reduced from 19.18 to 15.3% after oxygen annealing, assuming the total area under the curve of O 1 s 100%. This indicates that annealing decreased the oxygen or oxygen-related vacancies concentration and other defect states, which in turn lowered the dark current of the MSM PD fabricated on annealed β-Ga_2O_3 thin film.

A photoluminescence study was conducted to understand the origin of sub-band response of β-Ga_2O_3 thin films PDs. Figure 5 shows the PL spectra of as-grown and annealed β-Ga_2O_3 thin films measured at 77 K at an excitation wavelength of $\lambda_{excitation} = 270$ nm. Five distinct emission peaks appearing at 372, 391, 415, 440, and 475 nm were visible in both spectra. The UV emissions (372 and 391 nm) are intrinsic emissions of β-Ga_2O_3 and are attributed to the recombination of the self-trapped excitons [40–42]. Self-trapped excitons are created when an electron at the donor level (being formed by oxygen vacancies) is captured by a hole at the acceptor level (being formed by gallium vacancy (V_{Ga})), or a pair of gallium and oxygen vacancies (V_O, V_{Ga}). The blue emission (415, 440, and 490 nm) may originate from the recombination of a donor–acceptor pair (DAP) through tunneling, as suggested by theoretical studies [41, 42]. It has been reported previously that both the UV and blue emission depend on the concentration of oxygen vacancies [43]. The intensities of all the peaks are reduced for the annealed thin film as compared to those of the as-grown one. Such reduction in intensity after annealing can be attributed to the decrease in the concentration of oxygen or oxygen-related vacancies. Annealing under oxygen atmosphere promoted the annihilation of oxygen and oxygen-related vacancies which led to the reduction of the processes responsible for UV and blue emission.

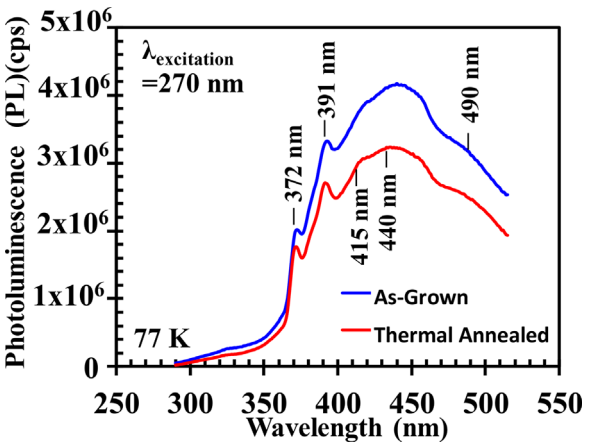

Figure 5 PL spectra of as-grown and thermal annealed β-Ga_2O_3 thin films measured at 77 K.

Time-dependent photoresponse of the PDs fabricated on as-grown and thermally annealed β-Ga_2O_3 thin films to a 250 nm UV illumination by on/off switching was evaluated under an applied bias of 1 V, as shown in Fig. 6. The devices exhibited an identical response (not shown) to UV light even after multiple cycles of illumination. This indicates the good reproducibility and robustness of the fabricated PD. The rise and decay edges of a PD usually consist of two components, a fast response component and a slow response component. The quantitative analysis of the process of the current rise and decay involves fitting of the photoresponse curve with a bi-exponential relaxation equation of the following type [32]:

$$I = I_o + Ae^{\frac{-t}{\tau_1}} + Be^{\frac{-t}{\tau_2}} \quad (1)$$

where I_o is the steady state photocurrent, t is the time, A and B are constants, and τ_1 and τ_2 are two relaxation time constants.

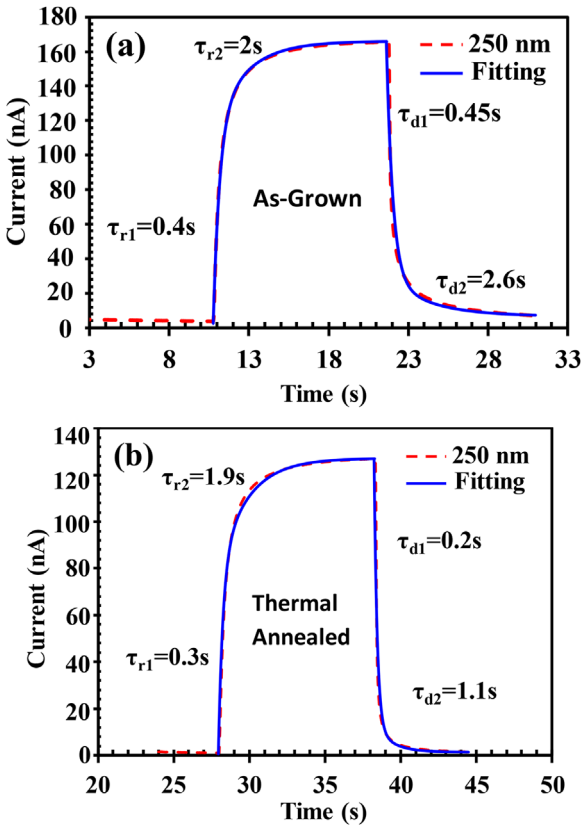

Figure 6 Experimental data for the rise/decay processes and the corresponding exponential fitting of the as-grown and thermal annealed β-Ga_2O_3 thin film photodetector to 250 nm illumination.

The photoresponse processes are well fitted as shown in Fig. 6(a and b), τ_r and τ_d are the time constants for the rise and decay edges, respectively. The fast-response component is generally attributed to the rapid change of the carrier concentration as soon as the UV light is turned on or off, while the slow-response component is caused by the carrier trapping/releasing due to the existence of defects in β-Ga_2O_3 thin films. For both types of devices, we did not observe any persistent photoconductivity (PPC) effects. The current decreased rapidly, close to the dark current value when the UV light source was turned off. The PD fabricated on a thermally annealed thin film exhibited a faster response to a 250 nm light than that of the as-grown one, which can be attributed to the reduction of oxygen and oxygen-related vacancies concentration in the β-Ga_2O_3 thin films. We observed that both the responsivity and a time-dependent photoresponse of PDs improved after thermal annealing. This might be due to the increase of depletion layer thickness resulting from the decrease of oxygen and oxygen-related vacancies. Such phenomena have been observed previously for β-Ga_2O_3 thin film based PDs deposited by laser MBE technology [1, 16].

4 Conclusions In summary, solar-blind PDs based on as-grown and annealed β-Ga_2O_3 thin films synthesized on c-plane sapphire by LPCVD were demonstrated. Annealing in an oxygen atmosphere significantly suppressed the oxygen-related defects of the β-Ga_2O_3 thin films leading to an enhanced device performance. The PD fabricated on an annealed β-Ga_2O_3 thin film exhibited a lower dark current and a higher out of band rejection ratio as compared to the one fabricated on an as-grown β-Ga_2O_3 thin film. The results indicate that annealing is an effective approach to fabricate high performance β-Ga_2O_3 thin film solar-blind PD.

Acknowledgement Part of the material characterization was performed at the Swagelok Center for Surface Analysis of Materials (SCSAM) at CWRU.

References

[1] D. Y. Guo, Z. P. Wu, Y. H. An, X. C. Guo, X. L. Chu, C. L. Sun, L. H. Li, P. G. Li, and W. H. Tang, Appl. Phys. Lett. **105**, 023507 (2014).
[2] S. Ahn, Y.-H. Lin, F. Ren, S. Oh, Y. Jung, G. Yang, J. Kim, M. A. Mastro, J. K. Hite, C. R. Eddy, Jr., and S. J. Pearton, J. Vac. Sci. Technol. B **34**, 041213 (2016).
[3] V. Kuryatkov, A. Chandolu, B. Borisov, G. Kipshidze, K. Zhu, S. Nikishin, H. Temkin, and M. Holtz, Appl. Phys. Lett. **82**, 1323 (2003).
[4] Z. G. Ju, C. X. Shan, D. Y. Jiang, J. Y. Zhang, B. Yao, D. X. Zhao, D. Z. Shen, and X. W. Fan, Appl. Phys. Lett. **93**, 173505 (2008).
[5] Y. Koide, M. Liao, and J. Alvarez, Diamond Relat. Mater. **15**, 1962 (2006).
[6] E. Monroy, F. Calle, J. A. Garrido, P. Youinou, E. Munoz, F. Omnes, B. Beaumont, and P. Gibart, Semicond. Sci. Technol. **14**, 685 (1999).
[7] X. Du, Z. Mei, Z. Liu, Y. Guo, T. Zhang, Y. Hou, Z. Zhang, Q. Xue, and A. Y. Kuznetsov, Adv. Mater. **21**, 4625 (2009).
[8] M. Liao, Y. Koide, and J. Alvarez, Appl. Phys. Lett. **87**, 022105 (2005).
[9] S. Kumar, C. Tessarek, G. Sarau, S. Christiansen, and R. Singh, Adv. Eng. Mater. **17**, 709 (2015).
[10] W. Feng, X. Wang, J. Zhang, L. Wang, W. Zheng, P. Hu, W. Cao, and B. Yang, J. Mater. Chem. C **2**, 3254 (2014).
[11] Y. Li, T. Tokizono, M. Liao, M. Zhong, Y. Koide, I. Yamada, and J.-J. Delaunay, Adv. Funct. Mater. **20**, 3972 (2010).
[12] X. Chen, K. Liu, Z. Zhang, C. Wang, B. Li, H. Zhao, D. Zhao, and D. Shen, Appl. Mater. Interfaces **8**, 4185 (2016).
[13] S. Oh, J. Kim, F. Ren, S. J. Pearton, and J. Kim, J. Mater. Chem. C **4**, 9245 (2016).
[14] Y. Qu, Z. Wu, M. Ai, D. Guo, Y. An, H. Yang, L. Li, and W. Tang, J. Alloys Compd. **680**, 247 (2016).
[15] F.-P. Yu, S.-L. Ou, and D.-S. Wuu, Opt. Mater. Express **5**, 1240 (2015).
[16] Y. H. An, D. Y. Guo, S. Y. Li, Z. P. Wu, Y. Q. Huang, P. G. Li, L. H. Li, and W. H. Tang, J. Phys. D: Appl. Phys. **49**, 285111 (2016).
[17] T. Oshima, T. Okuno, and S. Fujita, Jpn. J. Appl. Phys. **46**, 7217 (2007).
[18] S. Oh, Y. Jung, M. A. Mastro, J. K. Hite, C. R. Eddy, Jr., and J. Kim, Opt. Express **23**, 28300 (2015).

[19] R. Suzuki, S. Nakagomi, Y. Kokubun, N. Arai, and S. Ohira, Appl. Phys. Lett. **94**, 222102 (2009).
[20] T. Oshima, T. Okuno, N. Arai, N. Suzuki, S. Ohira, and S. Fujita, Appl. Phys. Express **1**, 011202 (2008).
[21] W.-Y. Kong, G.-A. Wu, K.-Y. Wang, T.-F. Zhang, Y.-F. Zou, D.-D. Wang, and L.-B. Luo, Adv. Mater. **28**, 10725 (2016).
[22] M.-Y. Tsai, O. Bierwagen, M. E. White, and J. S. Speck, J. Vac. Sci. Technol. A **28**, 354 (2010).
[23] M. Baldini, M. Albrecht, A. Fiedler, K. Irmscher, R. Schewski, and G. Wagner, ECS J. Solid State Sci. Technol. **6**, Q3040 (2017).
[24] H. Murakami, K. Nomura, K. Goto, K. Sasaki, K. Kawara, Q. T. Thieu, R. Togashi, Y. Kumagai, M. Higashiwaki, A. Kuramata, S. Yamakoshi, B. Monemar, and A. Koukitu, Appl. Phys. Express **8**, 015503 (2015).
[25] S. Rafique, L. Han, A. T. Neal, S. Mou, M. J. Tadjer, R. H. French, and H. Zhao, Appl. Phys. Lett. **109**, 132103 (2016).
[26] S. Rafique, L. Han, and H. Zhao, Phys. Status Solidi A **213**, 1002 (2016).
[27] S. Rafique, L. Han, M. J. Tadjer, J. A. Freitas, Jr., N. A. Mahadik, and H. Zhao, Appl. Phys. Lett. **108**, 182105 (2016).
[28] R. Suzuki, S. Nakagomi, and Y. Kokubun, Appl. Phys. Lett. **98**, 131114 (2011).
[29] M. Ai, D. Guo, Y. Qu, W. Cui, Z. Wu, P. Li, L. Li, and W. Tang, J. Alloys Compd. **692**, 634 (2017).
[30] P. Ravadgar, R.-H. Horng, S.-D. Yao, H.-Y. Lee, B.-R. Wu, S.-L. Ou, and L. W. Tu, Opt. Express **21**, 24599 (2013).
[31] G. C. Hu, C. X. Shan, N. Zhang, M. M. Jiang, S. P. Wang, and D. Z. Shen, Opt. Express **23**, 13554 (2015).
[32] D. Guo, Z. Wu, P. Li, Y. An, H. Liu, X. Guo, H. Yan, G. Wang, C. Sun, L. Li, and W. Tang, Opt. Mater. Express **4**, 1067 (2014).
[33] S. Nakagomi, T.-A. Sato, Y. Takahashi, and Y. Kokuban, Sens. Actuators A **232**, 208 (2015).
[34] S. Nakagomi, T. Momo, S. Takahashi, and Y. Kokubun, Appl. Phys. Lett. **103**, 072105 (2013).
[35] X. C. Guo, N. H. Hao, D. Y. Guo, Z. P. Wu, Y. H. An, X. L. Chu, L. H. Li, P. G. Li, M. Lei, and W. H. Tang, J. Alloys Compd. **660**, 136 (2016).
[36] S. Nakagomi and Y. Kokubun, J. Cryst. Growth **349**, 12 (2012).
[37] S. Yan, S. Ge, Y. Zuo, W. Qiao, and L. Zhang, Scr. Mater. **61**, 387 (2009).
[38] Y. An, S. Wang, L. Duan, J. Liu, and Z. Wu, Appl. Phys. Lett. **102**, 212411 (2013).
[39] A. Samariya, R. K. Singhal, S. Kumar, Y. T. Xing, S. C. Sharma, P. Kumari, D. C. Jain, S. N. Dolia, U. P. Deshpande, T. Shripathi, and E. Saitovitch, Appl. Surf. Sci. **257**, 585 (2010).
[40] T. Harwig and F. Kellendonk, J. Solid State Chem. **24**, 255 (1978).
[41] L. Binet and D. Gourier, J. Phys. Chem. Solids **59**, 1241 (1998).
[42] J. B. Varley, A. Janotti, C. Franchini, and C. G. Van De Walle, Phys. Rev. B **85**, 081109 (2012).
[43] E. G. Villora, M. Yamaga, T. Inoue, S. Yabasi, Y. Masui, T. Sugawara, and T. Fukuda, Jpn. J. Appl. Phys. **41**, L622 (2002).